Available online at www.sciencedirect.com
SCIENCE DIRECT®
Journal of Power Sources 124 (2003) 518–525
JOURNAL OF POWER SOURCES
www.elsevier.com/locate/jpowsour

Characterization of the lithium surface by infrared and Raman spectroscopies

C. Naudin, J.L. Bruneel, M. Chami, B. Desbat, J. Grondin, J.C. Lassègues*, L. Servant

Laboratoire de Physico-Chimie Moléculaire, UMR 5803, CNRS, Université Bordeaux I, 351 Cours de la Libération, 33405 Talence Cedex, France

Received 8 April 2003; received in revised form 27 June 2003; accepted 30 June 2003

Abstract

The chemical composition of the pristine passivation layer formed on the surface of commercial lithium foils has been investigated by polarization modulation infrared reflection absorption spectroscopy (PM-IRRAS) and confocal Raman microspectrometry (CRM). Carbonates and hydroxides are easily detected by PM-IRRAS and on-line non-destructive analysis could be envisaged with this technique or even with the simpler IRRAS technique in dry atmosphere. On the other hand, local heating under laser irradiation is difficult to avoid in CRM. It transforms carbonate species into lithium acetylides of the Li_2C_2 type characterized by a $\nu C{\equiv}C$ line at ca. 1845 cm^{-1}. This might explain an unexpected Raman line observed at 1830–1850 cm^{-1} in previous literature studies of the lithium/electrolyte interface or of the carbon/electrolyte interface in lithium-ion batteries.

Keywords: Lithium surface; Passivating layer; Raman; Infrared; Lithium carbonate; Lithium acetylide

1. Introduction

The lithium metal foils used as anode in lithium/polymer batteries are either provided by manufacturers or/and laminated to be assembled on-line with a polymer electrolyte film and a composite cathode film [1,2]. In all cases, chemical reactions of lithium with atmospheric gases take place and the lithium anode is always covered with an inorganic film, the thickness and chemical composition of which depend on the preparation and storage conditions. It is important to control the formation of this pristine film as it seems to influence the subsequent chemical reactions occurring at the lithium/electrolyte interface and ultimately the mechanisms of dendritic growth and the cycling efficiency of the battery [1–6]. Since lithium is a highly reactive metal, its surface composition has sometimes been deliberately modified, for example by treatment with CO_2 [7,8], HF [9] and other reactants [10] or by coating with polymers [11], in order to stabilize an interface of low resistivity and to improve the performances of the battery.

As far as commercial lithium foils are concerned, many studies have already been performed on the native passivating film and they generally conclude to the presence of an outer Li_2CO_3/LiOH layer of 1–20 nm thickness superimposed on a thicker Li_2O layer (10–100 nm) [12–15]. Most of these studies have used X-ray photoelectron spectroscopy (XPS) under high vacuum but some have been performed with other techniques such as ellipsometry [16] or vibrational spectroscopy [2,4–6,12]. In situ spectroscopic techniques in a controlled atmosphere are in principle well adapted for an easy control of commercial lithium foils. The goal of the present study is to see whether IR and Raman spectroscopies can provide a non-destructive and fast way of testing the quality of the lithium anode just before it is assembled with the other battery elements. As the passivating layer is very thin, we have used polarization modulation infrared reflection absorption spectroscopy (PM-IRRAS) and confocal Raman microspectrometry (CRM) as probing techniques.

2. Experimental

2.1. Materials

Commercial lithium foils of 50 and 100 μm thicknesses coming from two companies (A and B) have been investigated either as-received under a dry argon atmosphere or after exposure for several hours to an air atmosphere containing CO_2 and 300 ppm H_2O (Table 1). All these samples are kept in hermetic glass containers and stored inside a dry

* Corresponding author. Tel.: +33-5-56-846355; fax: +33-5-56-848402.
E-mail address: jc.lassegues@lpcm.u-bordeaux1.fr (J.C. Lassègues).

0378-7753/$ – see front matter © 2003 Elsevier B.V. All rights reserved.
doi:10.1016/S0378-7753(03)00798-5

Table 1
List of the investigated lithium foils

Source	Lithium thickness (μm)	Stored under argon	Exposed to dry air
A	100	A100i	A100d
B	100	B100i	B100d
B	50	B50i	B50d

Samples A have been extruded in a $Ar + CO_2$ atmosphere and sample B in a pure Ar atmosphere. They have then been stored under dry argon (i) or exposed during several hours to "dry" air containing 300 ppm H_2O (d). Sample B50 is obtained from sample B100 by a second laminating process.

box under argon (2 ppm O_2 and H_2O). Pieces of about 1 cm diameter are introduced either in cell (a) for the PM-IRRAS experiments or in cell (b) for the CRM experiments (Fig. 1). These cells are equipped with taps that allow evacuation and introduction of various gases. Dilithioacetylene, Li_2C_2 has been synthesized at the Centre de Datation par le Radiocarbone (Université Claude Bernard Lyon 1) by heating lithium in presence of CO_2 at 650 °C. The exothermic reaction gives Li_2C_2 and Li_2O.

2.2. Spectroscopic approaches

The principle of the PM-IRRAS technique has been described elsewhere [17]. Briefly, infrared reflection absorption spectroscopy (IRRAS) on a metal surface at grazing incidence and using a polarized IR beam takes advantage of the strong anisotropy of the electric field in the vicinity of the metal surface: the p-polarized light, contained in the incidence plane, interacts much more strongly with the surface vibrations than the s-polarized one perpendicular to the incidence plane. Information can then be obtained on the molecular orientation within a thin film on the metal since the p-polarized light privileges vibrational modes having their transition moments perpendicular to the surface. When the polarization of the incident beam is modulated very quickly between the s and p components (PM-IRRAS), a differential reflectivity is measured in real time and all isotropic absorptions (external H_2O and CO_2 gases) and instrumental variations are cancelled. PM-IRRAS is thus a much more sensitive technique than IRRAS in order to analyze very thin layers on a metal. This has already been illustrated on lithium by Morigaki and Ohta [12].

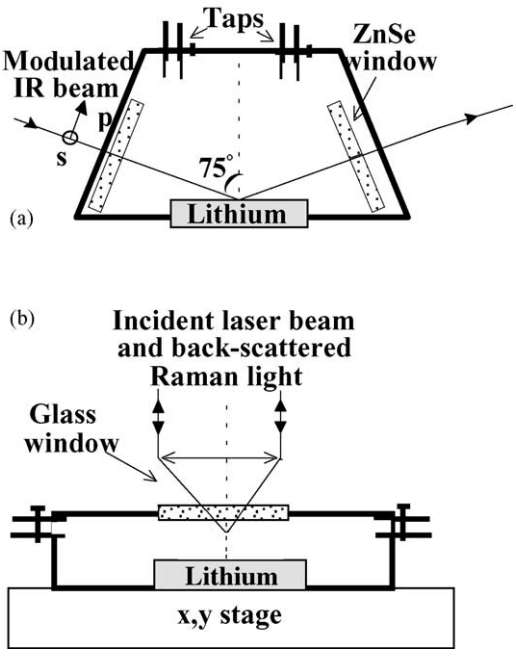

Fig. 1. Schematic drawing of the cells used for the PM-IRRAS (a) and CRM (b) experiments. Cell (b) is installed on a x, y computer controlled stage below the microscope. It can also be moved vertically along z by steps of 1 μm.

The IR experiments have been performed on a FT-IR Nexus (Nicolet) spectrometer using a spectral resolution of 4 cm^{-1} and the external parallel beam available on this spectrometer. The optical set-up involving a polarizer, a photoelastic modulator, the sample and the detector (liquid nitrogen-cooled MCT detector) is installed on an external bench in order to measure the sample reflectance at a grazing incidence of 75° either in IRRAS or in PM-IRRAS. The path-length between the source and the detector is about 1 m and a sample area of ca. 0.3 cm × 1.2 cm is illuminated. The modulation frequency in PM-IRRAS is generally chosen at 1550 cm^{-1} and 200 scans are co-added.

The principle of the CRM technique has also been described previously [19]. It allows surface and in-depths Raman analyses to be performed with a micrometric spatial resolution. Experiments are performed with a Labram 1B spectrometer (Dilor, Jobin-Yvon) using its He/Ne (632.8 nm) laser or a Ar/Kr 2018 Spectra-Physics laser (457.9, 514.5 or 725.5 nm) and a 600 lines/mm grating (spectral resolution ca. 8 cm^{-1} at $\lambda_0 = 514.5$ nm). The laser is focussed on the sample through the microscope with a 50× Olympus objective of 0.55 numerical aperture (NA) and 8.1 mm working distance. For a given objective, the radial resolution for experiments on the lithium surface and the axial resolution for in-depth experiments at the electrolyte/lithium interface depend on the diameter of the confocal pin-hole and of the incident wavelength as previously reported [19]. However, these resolutions are not critical in the present study, except in the case of in-depth analyses at the polymer electrolyte/lithium interface. Using a confocal pin-hole of 250 μm at $\lambda_0 = 514.5$ nm, the axial resolution at this interface is ca. 5 μm for a polymer electrolyte of 50 μm thickness and ca. 1.5 refractive index. For surface analyses on bare lithium foils, the confocal pin-hole is set at 1000 μm in order to increase the Raman light output. A more important aspect is the laser irradiance at the sample. Indeed, it has been found that heating effects produce chemical transformations on the lithium surface for irradiances higher than ca. 1 $mW/\mu m^2$. The laser irradiance is evaluated by measuring first the laser power below the objective of the microscope with a Coherent hand-held laser power meter and then

considering an irradiated spot of ca. $1.22\lambda_0$/NA diameter. For $\lambda_0 = 514.5$ nm and NA = 0.55, the critical irradiance of 1 mW/μm^2 is reached with a laser power at the sample of only 1 mW.

2.3. Spectral data treatments

The IRRAS spectra are presented in terms of a pseudo-absorbance $A = 1 - R_p(\mathrm{Li})/R_p(\mathrm{m})$ where $R_p(\mathrm{m})$ and $R_p(\mathrm{Li})$ are the reflectivities of the p-polarized light by a gold mirror and by the lithium surface, respectively. The PM-IRRAS spectra are first obtained under the form:

$$S = \frac{CJ_2(\Phi_0)(R_p - R_s)}{[J_0(R_p - R_s) \pm (R_p + R_s)]} \quad (1)$$

where C is a constant amplification factor determined by the experimental conditions and J_0 and $J_2(\Phi_0)$ are Bessel functions of order 0 and 2, respectively. At grazing incidences on a metal surface, $J_0(R_p - R_s) \ll (R_p + R_s)$ in Eq. (1) as both R_p and R_s are close to 1. Nevertheless, the experimental parameters C, J_0 and J_2 can be evaluated in a separate experiment performed with a second polarizer placed between the sample and the detector. The two polarizers are oriented in the ss ($R_p = 0$) or sp ($R_s = 0$) configurations in order to measure:

$$S_{ss} = \frac{CJ_2}{J_0 - 1} \quad (2)$$

$$S_{sp} = \frac{CJ_2}{J_0 + 1} \quad (3)$$

By combining Eqs. (1)–(3), it is possible to extract the normalized differential reflectivity:

$$\frac{\Delta R}{R} = \frac{R_p - R_s}{R_p + R_s} \quad (4)$$

which can be transformed into the $1 - R_p/R_s = (2\Delta R/R)/(\Delta R/R - 1)$ representation if necessary.

The CRM spectra have been processed with the Labspec program installed on the Labram spectrometer and with the Galactic GRAMS/32 program.

3. Results and discussion

3.1. Infrared spectra

The PM-IRRAS spectra of the six lithium samples reported in Fig. 2 are characteristic of a carbonate species with the intense ν_2 and ν_3 absorption bands and a weak ν_1 absorption at ca. 1089 cm^{-1}. The ν_2 and ν_3 intensities provide a qualitative indication of the relative amount of carbonate on the different films: 100 μm thick B foils extruded under argon atmosphere have a slightly thinner carbonate layer than A foils extruded under argon/CO_2 atmosphere; 50 μm thick foils produced from the 100 μm ones by a second laminating process exhibit a thicker carbonate layer. Finally, exposition to dry air increases systematically the carbonate thickness.

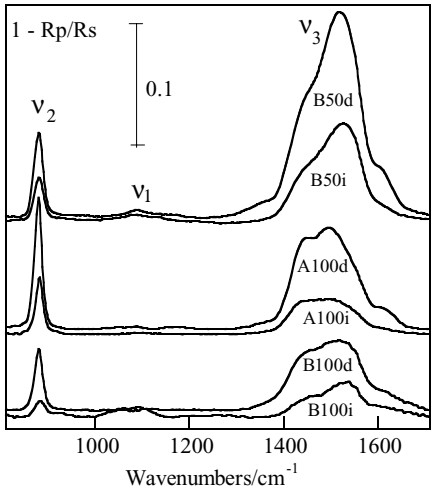

Fig. 2. PM-IRRAS spectra of the various lithium samples are described in the text and in Table 1. The main carbonate absorptions ν_2 and ν_3 are indicated together with the very weakly active ν_1 mode. Scans (500) have been co-added.

It is well established that the IR reflection spectra of thin solid films as a function of the incidence angle exhibit changes in the peak positions and shapes coming from a variable contribution of the transverse optic (TO) and longitudinal optic (LO) components of a given vibration. For Li_2CO_3 (C_{2h}^6 space group) the TO and LO components have been found at 1420 and 1606 cm^{-1} for ν_3, 859 and 867 cm^{-1} for ν_2, respectively, whereas a weak ν_1 (TO) band is reported at 1088 cm^{-1} [21]. The spectra of the thin Li_2CO_3 layer formed on the lithium surface correspond only qualitatively to the above observations (Fig. 2). The ν_2 vibration gives an asymmetric band centred at ca. 880 cm^{-1}. The ν_3 band profile is quite variable from one sample to another and more complex than expected: in addition to the intense components at 1454 and 1530 cm^{-1} that can be assigned to the TO and LO modes, respectively, shoulders are observed at ca. 1635 and 1375 cm^{-1}. When the sample is exposed to CO_2, the ν_3 components and in particular the 1635 cm^{-1} shoulder are more intensified than the ν_2 profile (Fig. 3). In the experiment reported in Fig. 3, the spectra have been recorded down to 700 cm^{-1} and up to 3800 cm^{-1} in order to see whether the growing 1635 cm^{-1} band is associated to some other new absorptions. A weak and narrow line corresponding to the stretching vibration of the hydroxyl group in LiOH is observed at 3677 cm^{-1}; its intensity is slightly increased by exposure to CO_2 but no additional absorption is detected that could be assigned to the νOH vibration of hydrogenocarbonate $LiHCO_3$. The LiOH content increases because CO_2 gas is not completely free from H_2O and, in addition, degassing of the metallic parts of the cell certainly occurs for such long storing times. The lithium foils that were never exposed to "dry" air exhibit much less intense νOH bands. The only new absorption in Fig. 3 occurs at

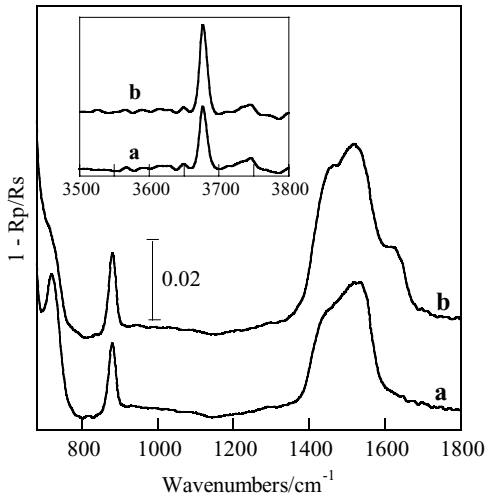

Fig. 3. PM-IRRAS spectra of lithium B100d before (a) and after (b) exposition to CO_2 gas during 19 h. The νOH band of LiOH is reported in the inset.

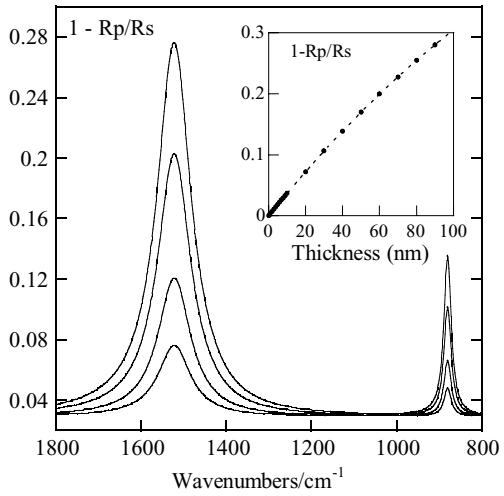

Fig. 4. Simulated PM-IRRAS spectra of Li_2CO_3 (see text) for thicknesses of 5, 10, 20 and 30 nm. The calibration of the ν_2 band intensity as a function of thickness is reported in the inset.

720 cm^{-1} and can be assigned to the ν_4 mode of Li_2CO_3. Finally, the 1635 cm^{-1} absorption does not clearly correspond to either hydrogenocarbonate or oxalate anions. It might be due to CO_2 molecules in strong interaction with surface oxygen groups to give unidentate or bidentate complexes of the Li–O–COO–Li or $OC(O–Li)_2$ type.

Returning to the PM-IRRAS spectra of the pristine passivation layer (Fig. 2), we have tried to model the experimental profiles of the carbonate layer in order to evaluate its mean thickness. We have applied the simulation program developed by Buffeteau and co-workers [18,20] to the multilayer system air/carbonate/lithium, the inner Li_2O layer being neglected as its vibrations do not contribute to the investigated spectral region. Within the 800–1800 cm^{-1} spectral range, the lithium substrate has been supposed isotropic with a constant refractive index $\check{n} = n + ik = 3.66 + i38$ corresponding to the literature data at 0.15 eV (1210 cm^{-1}) [22]. The frequency dispersion of the n and k optical constants of Li_2CO_3 is calculated according to the model of dielectric constant described by Balkansky [23] using the experimentally determined ω_{TO} and ω_{LO} angular frequencies of the transverse optic and longitudinal optic modes, respectively, and the corresponding full-widths at half-maximum (FWHM) γ_{TO} and γ_{LO}. The experimental spectra are fitted with gaussian components and the results (in cm^{-1}) are: $\nu_{2(TO)} = 866$, $\gamma_{2(TO)} = 20$; $\nu_{2(LO)} = 880$, $\gamma_{2(LO)} = 20$; $\nu_{3(TO)} = 1441$, $\gamma_{3(TO)} = 91$; $\nu_{3(LO)} = 1522$, $\gamma_{3(LO)} = 91$. Simulations are run at an incidence angle of 75° for Li_2CO_3 films thicknesses varying in the 0–100 nm range and assuming random orientations of the carbonate groups, i.e. isotropic optical constants. The simulated PM-IRRAS spectra in the $1 - R_p/R_s$ form are reported in Fig. 4. The ν_2 profile is rather well reproduced but the ν_3 profile is dominated by the LO component and reproduces only approximately the experimental profiles that exhibit a better separated TO component (Fig. 2). This is not too surprising if one considers the large number of hypotheses made in the calculation. Indeed, the surfaces and interfaces of the $Li/Li_2O/Li_2CO_3$ system are certainly rather rough with a possible interpenetration of the Li_2O and Li_2CO_3 phases. The optical contribution of the Li_2O phase has been neglected and it is quite likely that the Li_2CO_3 layer has not a constant thickness but is rather formed of clusters of variable size. Finally, the carbonate groups in these clusters, although more disordered than in the Li_2CO_3 crystal, may adopt some preferential orientation depending on the preparation conditions. All these features are expected to affect the relative intensities and splittings of the TO/LO components. The results of Fig. 2 indicate effectively that the relative intensities of the ν_2 and ν_3 bands vary from one sample to another. For example, the ν_3 maximum intensity is stronger than the ν_2 one for the calculated spectra as for the B samples whereas the reverse situation is observed for the A samples processed in an argon/CO_2 atmosphere. One can infer that B samples satisfy better the isotropic orientation hypothesis. Since the transition moment of the ν_2 vibration is perpendicular to the carbonate plane and the transition moment of the ν_3 vibration is contained in this plane, samples A would have a preferential orientation of the carbonate groups parallel to the lithium surface. The relative intensity of the TO and LO components in the ν_3 profile varies also from one sample to another. The mean TO/LO splitting is only ca. 81 cm^{-1}, compared to 186 cm^{-1} in the crystal [21] and this can be related to the limited sizes of the Li_2CO_3 grains. So, there are several experimental evidences of particular features of the actual Li_2CO_3 layers that are not taken into account in the calculation. We have not tried to develop more sophisticated models (anisotropic optical constants, non-uniform thickness, etc.) because too many unknown parameters would be involved. A mean carbonate thickness has rather been evaluated from

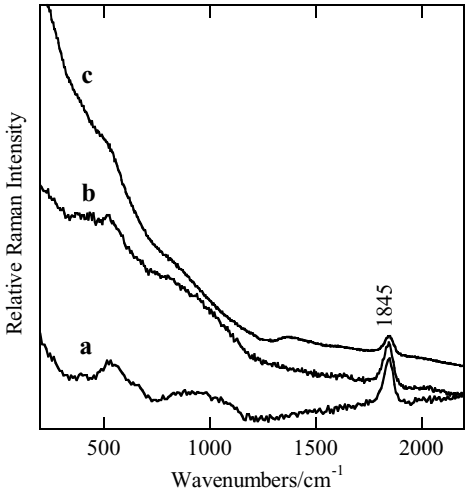

Fig. 5. CRM spectra of lithium A100i recorded with a 50×, NA = 0.55 objective and an incident wavelength of 514.5 nm and (a), 632.8 nm (b) and 752 nm (c). The laser irradiance at the sample is ca. 1 mW/μm^2.

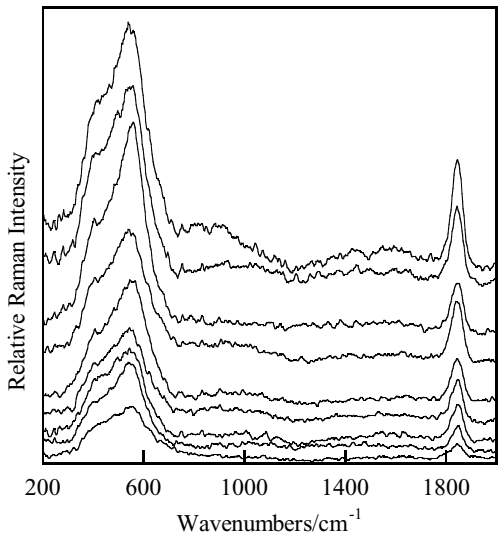

Fig. 6. CRM spectra of lithium B100d recorded at nine different points with an incident wavelength of 632.8 nm, a 50×, NA = 0.55 objective and P ca. 1 mW/μm^2. A baseline correction has been applied for a more convenient comparison.

the calculated intensity of the ν_2 band reported in the inset of Fig. 4. Using this calibration curve, the experimental ν_2 intensities of Fig. 2 yield the following sequence: B100i (3 nm) < B50i (9 nm) < A100i (11 nm) ≈ B100d (12 nm) < B50d (18 nm) < A100d (28 nm). These thicknesses are in good agreement with those found by other techniques on commercial lithium foils [12–15] but their absolute values have to be considered with care in view of all the limitations described above. It can nevertheless be safely concluded that sample B100i has the thinner carbonate passivating layer.

3.2. Raman spectra

A given lithium sample (A100i) has first been studied with several exciting wavelengths. No Raman spectrum is detected until the laser irradiance at the sample has reached a limiting value of about 1 mW/μm^2. Then, it can be seen in Fig. 5 that a relatively narrow band appears at 1845 cm^{-1}, accompanied by broader bands centred at about 550 and 410 cm^{-1}. All these features correspond to true Raman excitations as their positions do not depend on the incident wavelength. On the other hand, they are situated on a background having quite a variable sloping line. This background comes from fluorescence effects that are frequency shifted as a function of the wavelength. In the following presentations the Raman spectra are corrected for this fluorescence background. If the sample is probed on nine different points for a given incident wavelength and power of the laser, quite variable intensities are observed for the Raman features at 1855 and around 500 cm^{-1} (Fig. 6). This confirms that the passivation layer has a rather in-homogeneous thickness. After averaging the nine spectra of a given sample, a comparison of the six samples leads to a classification roughly similar to that observed in PM-IRRAS (Fig. 7). In particular, sample B100i gives the weakest signals and should present in average the thinnest passivating layer. However, the assignment of the observed Raman features is not straightforward. The broad bands centred at about 550 and 410 cm^{-1} could originate from a Li_2O disordered phase but there is no indication of any characteristic line of LiOH and Li_2CO_3 although their presence has been ascertained by PM-IRRAS. Moreover, the spectra of Fig. 7 do not change when lithium is exposed to N_2, O_2, CO_2 or CO atmospheres. The pristine carbonate layer should give a relatively narrow ν_1 line at 1090 cm^{-1} but this layer is either too thin to be detected by CRM or is chemically transformed by local heating of the laser. The latter hypothesis is more probable as it has

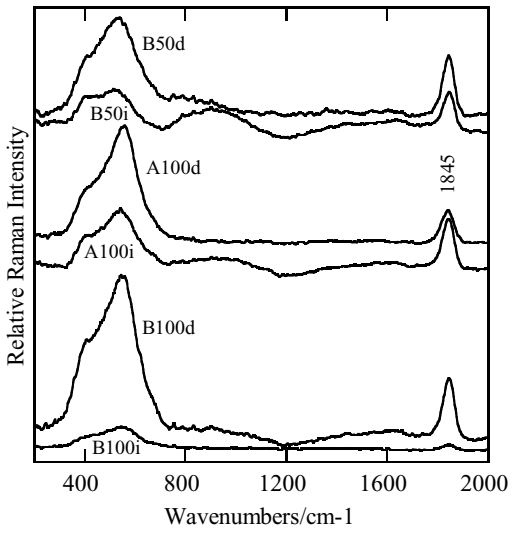

Fig. 7. CRM spectra of the six different lithium samples recorded as in Fig. 6 but after averaging in each case over nine different points.

been remarked that a coloured spot appears after each experiment at the irradiated surface independently of the incident wavelength. The key parameter is obviously the laser power. When it is very low, no coloured spot is observed on the surface but no Raman spectrum can be recorded. When the laser power is progressively increased, the Raman spectrum previously described is obtained but a coloured spot is then observable on the irradiated surface and it becomes darker when the laser power is increased. At even higher laser power, lithium melts, which means that the temperature of 180 °C has been locally reached. This is illustrated in Fig. 8. Lithium B50d has been studied as a function of laser power and time at $\lambda_0 = 514.5$ nm. The typical spectrum reported in Fig. 8a is obtained only for a laser irradiance P larger than ca. 1 mW/μm^2 and smaller than ca. 5 mW/μm^2. It is unchanged as a function of exposition time and involves essentially the 1845 cm^{-1} line and the Li_2O band near 500 cm^{-1}. When the incident irradiance is increased above 5 mW/μm^2, the intensity of the 1845 cm^{-1} line decreases as a function of time and new features appear at lower frequency. At $P =$ 50 mW/μm^2, spectrum b in Fig. 8 is obtained after only 20 s. It exhibits new broad bands at about 1580 and 1360 cm^{-1} accompanied by a narrower line at 1072 cm^{-1}. They can easily be assigned to the so-called G and D bands of carbon [24] and to the ν_1 CO_3^{2-} vibration of lithium carbonate, respectively. After 350 s, spectrum c in Fig. 8 indicates that the 1845 cm^{-1} line has vanished whereas the carbon band intensities have strongly increased. Finally, after 1200 s, carbon is accompanied by a large amount of carbonate and the Li_2O features are still present (Fig. 8d). Observation of the laser spot on the lithium foil at the end of the experiment reveals local lithium melting. However, this melting does not propagate very far away from the laser irradiated zone as shown by the spectra of the lithium surface recorded on various points around the spot.

A second kind of experiment has then been undertaken with the lithium foil being covered by a ca. 50 μm thick polymer electrolyte layer. The polymer electrolyte is a complex of poly(ethylene oxide) (PEO) with lithium bis-(trifluoromethanesulphone)imide $LiN(SO_2CF_3)_2$(LiTFSI) of O/Li = 20 stoichiometry [25]. In-depth analysis can be performed starting from the air/electrolyte interface down to the electrolyte/lithium interface [19]. In this experiment, the electrolyte spectrum provides an internal reference for the observation of the interface as the normalization to some bands of PEO (for example in the δCH_2 region) compensates the overall decrease of intensity that occurs when the penetration depth increases [19]. The laser irradiance has been set at 1 mW/μm^2 and Raman spectra have been recorded as a function of irradiation time. The results reported in Fig. 9 show that the 1845 cm^{-1} line increases first very quickly before reaching a plateau after 1000 s. At the end of these two experiments, a spot is evidenced on the lithium surface but no supplementary bands originating from a degradation of the salt or polymer are detected.

After these two experiments, it can be concluded that the 1845 cm^{-1} line results from local degradation by heating of species initially present on the lithium surface. Further heating leads to elementary carbon and carbonates, which means that the precursors do contain carbon and oxygen atoms. The main problem is then to assign the 1845 cm^{-1} line which is situated in a rather unusual spectral range: it cannot be associated to C–O, C=O, C=C or CH_2 groups; N=N or N≡N groups are also unlikely as exposure to gaseous nitrogen

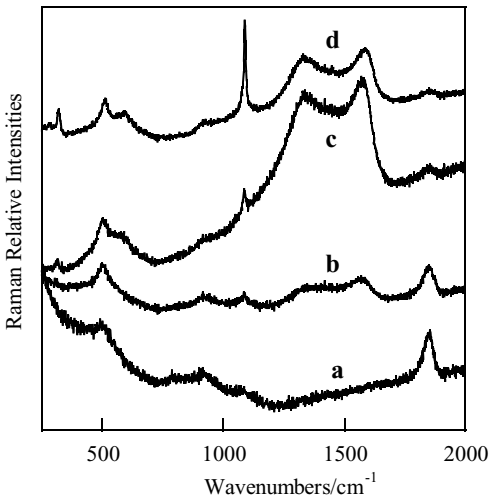

Fig. 8. CRM spectra recorded continuously on lithium B50d with $\lambda_0 = 514.5$ nm and a 50×, NA = 0.55 objective. Spectrum a is obtained for a laser irradiance of 5 mW/μm^2. Spectra b, c and d are obtained after 20, 350 and 1200 s, respectively, under a laser irradiance of 50 mW/μm^2. Each spectrum is recorded during 5 s and the intensity of spectrum a has been multiplied by 4 for a more convenient comparison.

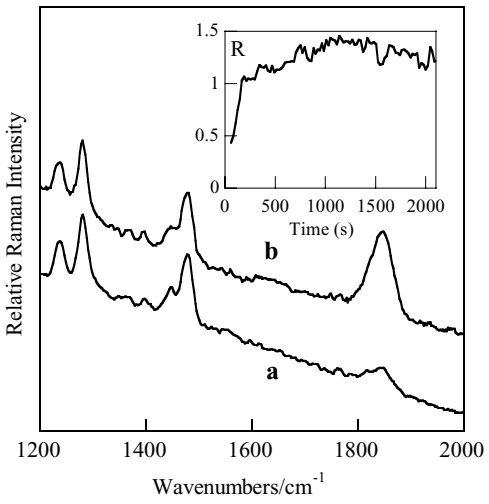

Fig. 9. CRM spectra recorded at the interface between lithium B100d and $P(EO)_{20}$, LiTFSI at $\lambda_0 = 632.8$ nm with a constant laser irradiance of 1 mW/μm^2, a 50×, NA = 0.55 objective and an accumulation time of 20 s per spectrum. Two examples of spectra obtained after 40 s (a) and 2000 s (b) are reported but continuous recording has been performed as a function of time. The evolution of the intensity ratio $R = A_{1845}/A_{1480}$ is given in the inset. A_{1845} and A_{1480} are the integrated intensities of the 1845 cm^{-1} acetylide band and of the 1480 cm^{-1} PEO band, respectively.

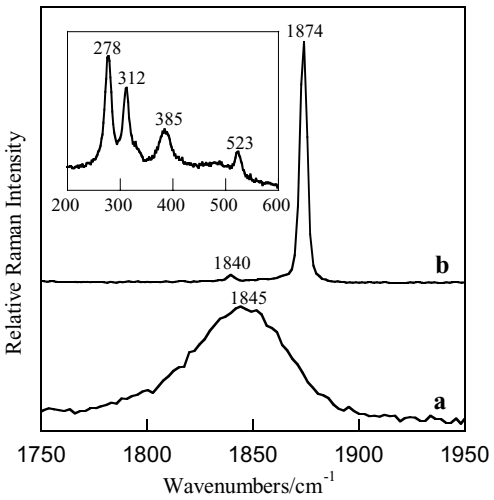

Fig. 10. Comparison of the CRM spectra of synthesized Li_2C_2 (a) and of the lithium surface (b) in the 1700–2000 cm^{-1} region. The low-frequency spectrum of Li_2C_2 is reported in the inset.

does not modify the 1845 cm^{-1} line intensity. According to the IR results, the more abundant species on the unperturbed lithium surface are carbonates. It is also known since a long time that lithium metal heated in a stream of CO_2 gives dilithioacetylene [26]. Therefore, we assign the 1845 cm^{-1} line to the stretching vibration of a C≡C group. The Raman spectrum of Li_2C_2 synthesized by heating lithium at 600 °C in the presence of CO_2 gas is compared in Fig. 10 to the profile of the 1845 cm^{-1} line. Solid Li_2C_2 gives effectively a very intense and narrow νC≡C line at 1874 cm^{-1} accompanied by a much weaker feature at 1840 cm^{-1} coming from the $\nu^{12}C\equiv^{13}C$ vibration according the expected frequency and intensity ratios for $^{12}C/^{13}C$ natural abundance (Fig. 10b). It can be admitted that the much broader 1845 cm^{-1} line (Fig. 10a) comes from a more disordered acetylide species of limited size on the lithium surface. The formation of other species containing a C≡C bond cannot be completely excluded. Alkali metals dissolved in ammonia have for example been shown to react with CO_2 to give a stable acetylenediolate salt Li–O–C≡C–O–Li [27]. However, if this species was formed, it should give other intense Raman lines in the 600–1800 cm^{-1} region. So, the formation of Li_2C_2 remains the more likely hypothesis since its Raman spectrum (Fig. 10b) does not exhibit any signal between 1800 cm^{-1} and the four lines at 523, 385, 312 and 278 cm^{-1} represented in the inset. The less intense 523 cm^{-1} component comes certainly from Li_2O which is known to be formed in the Li_2C_2 synthesis. We conclude that heating of the carbonate species initially present on the lithium surface gives first a transformation of Li_2CO_3 into Li_2C_2 and O_2^{2-}(Li_2O), then Li_2C_2 is decomposed into Li, carbonate and elemental carbon. It is noteworthy that a pure Li_2CO_3 sample submitted to the same levels of laser irradiance is not decomposed and gives a normal Raman spectrum of carbonate. The transformation into Li_2C_2 occurs only at the interface between carbonate and lithium metal.

As far as the characterization of the lithium surface is concerned, the conclusion of the CRM study is a rather pessimistic one since Raman signals are only obtained once a degradation reaction has occurred. However, these results can be helpful to understand several unexplained observations reported in the literature. In situ Raman studies at the graphite/electrolyte interface of lithium-ion batteries [28], at the lithium/gel electrolyte interface of a Li/poly(acrylonitrile)-$LiClO_4$-EC-PC/Li symmetric cell [29] or at the lithium/liquid electrolyte interface of a Li/$LiPF_6$-PC/Li symmetric cell [6], report the presence of a new intriguing line at 1830–1850 cm^{-1}. Some of the authors discuss the possible origin of this line [28,29] but no explanation is really satisfactory. We believe that a acetylide species formed by heating under the laser beam is involved in all cases. If this interpretation is correct, the observation of a line at ca. 1850 cm^{-1} constitutes a useful diagnostic for future Raman studies at the lithium/electrolyte interface.

By comparison with the CRM technique, PM-IRRAS is non-destructive but the available spectral range is limited to above 800 cm^{-1}. The Li_2O or Li_3N compounds cannot be detected since their vibrations occur below 600 cm^{-1}. Actually, the PM-IRRAS spectra are dominated by the carbonate absorptions and if the lithium samples have been kept in strictly anhydrous conditions, the νOH band of LiOH at 3677 cm^{-1} is even absent. Another limitation of PM-IRRAS arises from the rather large surface covered by the incident IR beam (ca. 0.3 cm^2) preventing in-homogeneities of thickness and composition to be analyzed. Keeping in mind these limitations, let us emphasize however that relatively fast and

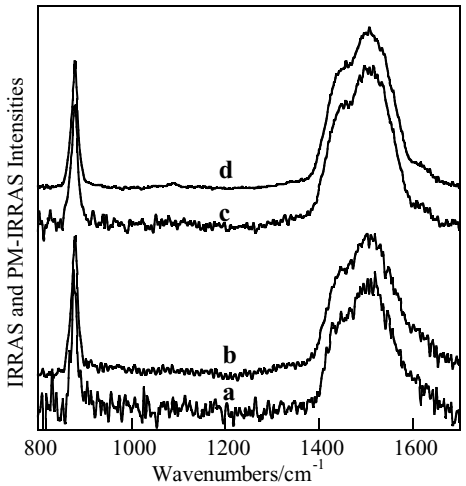

Fig. 11. Comparison of the IRRAS and PM-IRRAS spectra of lithiumB100i contained in cell (A) of Fig. 1. The IRRAS spectrum of a gold mirror has first been recorded with p-polarized light and used as a background for the IRRAS spectra of the lithium recorded in 2 scans (a) or 50 scans (b) with 0.6 s per scan. Then, without moving the cell, the incident light has been modulated between the p- and s-polarizations to obtain the PM-IRRAS spectra in 2 scans (c) or 50 scans (d) with 1.5 s per scan.

non-destructive on-line analysis of the lithium surface could be envisaged. If this analysis is to be performed in dry atmosphere, the simpler IRRAS technique may even be sufficient. This is illustrated in Fig. 11 where lithium B100i has been successively studied by IRRAS and PM-IRRAS. The atmospheric H_2O and CO_2 absorptions are well compensated in IRRAS and a reasonably good spectrum can be obtained in a few seconds. Nevertheless, the PM-IRRAS recorded in 3 s (Fig. 11c) has a better signal-to-noise than the IRRAS spectrum recorded in 30 s (Fig. 11b).

4. Conclusion

PM-IRRAS is a very well adapted non-destructive technique to detect carbonate and hydroxide species composing the lithium passivating layer. The simpler IRRAS technique may even be sufficient for on-line characterization of the lithium surface provided the experiment is performed in dry atmosphere. CRM does not detect the carbonates and hydroxides but reveals indirectly the presence of the former by a line at 1845 cm^{-1} which results from their transformation into species containing a C≡C bond (likely to be Li_2C_2) under the laser. This information is useful as it provides an explanation for the 1845 cm^{-1} Raman line being observed in many other situations at the lithium/electrolyte interface or at the carbon/electrolyte interface in lithium-ion batteries. Let us also recall that once the operating conditions are controlled to avoid degradation by laser heating, CRM keeps the unique advantage of in-depth analysis down to the electrolyte/lithium interface [19]. However, the sensitivity of normal Raman is rather limited and SERS effects would be very helpful to characterize the SEI [5].

Acknowledgements

The authors are grateful to J. Evin of the Centre de Datation par le Radiocarbone, Université Claude Bernard Lyon 1, for the gift of a Li_2C_2 sample and to Clare Edwards for her experimental help.

References

[1] D. Fauteux, Lithium electrodes in polymer electrolytes, in: T. Osaka, M. Datta (Eds.), Energy Storage Systems for Electronics, Gordon and Breach, Amsterdam, 2000.
[2] D. Aurbach, J. Power Sources 89 (2000) 206.
[3] C. Brissot, M. Rosso, J.-N. Chazalviel, S. Lascaud, J. Power Sources 81–82 (1999) 925.
[4] H. Li, Y. Mo, N. Pei, X. Xu, X. Huang, L. Chen, J. Phys. Chem. B 104 (2000) 8477.
[5] G. Li, H. Li, Y. Mo, L. Chen, X. Huang, J. Power Sources 104 (2002) 190.
[6] P.C. Howlett, D.R. MacFarlane, A.F. Hollekamp, J. Power Sources 5076 (2002) 1.
[7] T. Osaka, T. Momma, T. Tajima, Y. Matsumoto, J. Electrochem. Soc. 142 (1995) 1057.
[8] H. Gan, E.S. Takeuchi, J. Power Sources 62 (1996) 45.
[9] S. Shiraishi, K. Kanamura, Z.I. Takehara, J. Appl. Electrochem. 29 (1999) 869.
[10] J.S. Sakamoto, F. Wudl, B. Dunn, Solid State Ionics 144 (2001) 295.
[11] R.N. Mason, M. Smith, T. Andrews, D. Teeters, Solid State Ionics 118 (1999) 129.
[12] K. Morigaki, A. Ohta, J. Power Sources 76 (1998) 159.
[13] G. Zhuang, Y. Chen, P.N. Ross, Surf. Sci. 418 (1998) 139.
[14] K. Naoi, M. Mori, M. Inoue, T. Wakabayashi, K. Yamauchi, J. Electrochem. Soc. 147 (2000) 813.
[15] I. Ismail, A. Noda, A. Nishimoto, M. Watanabe, Electrochim. Acta 46 (2001) 1595.
[16] F. Kong, F. Mc Larnon, J. Power Sources 89 (2000) 180.
[17] T. Buffeteau, B. Desbat, J.M. Turlet, Appl. Spectrosc. 45 (1991) 380.
[18] S. Giasson, T. Palermo, T. Buffeteau, B. Desbat, J.M. Turlet, Thin Solid Films 252 (1994) 111.
[19] J.L. Bruneel, J.C. Lassègues, C. Sourisseau, J. Raman Spectrosc. 33 (2002) 815.
[20] T. Buffeteau, B. Desbat, Appl. Spectrosc. 43 (1989) 1027.
[21] M.H. Brooker, J.B. Bates, J. Chem. Phys. 54 (1971) 4788.
[22] M. Rasigni, G. Rasigni, J. Opt. Soc. Am. 67 (1977) 54.
[23] M. Balkansky, in: Abeles (Ed.), Optical Properties of Solids, North-Holland, Amsterdam, 1972 (Chapter 8).
[24] F. Salver-Disma, G. Fahri, C. Guéry, J.M. Tarascon, J.L. Bruneel, J.C. Lassègues, Mol. Cryst. Liqu. Cryst. 310 (1998) 211.
[25] I. Rey, J.C. Lassègues, J. Grondin, L. Servant, Electrochim. Acta 43 (1998) 1505.
[26] P. Pascal, Masson et Cie Nouveau (Ed.), Traité de Chimie minérale, Tome II, Paris, 1966, pp. 137–138.
[27] E. Weiss, W. Büchner, Z. Anorg. Allg. Chem. 330 (1964) 251.
[28] J.C. Panitz, F. Joho, P. Novák, Appl. Spectrosc. 53 (1999) 1188.
[29] D. Ostrovskii, P. Jacobsson, J. Electrochem. Soc. 149 (2002) A662.